RSC Advances

ARTICLE TYPE

Facile Thermal Annealing of Graphite Oxide in Air for Graphene with Higher C/O Ratios

Suyun Tian[a,b], Jing Sun[b], Siwei Yang[b], Peng He[b], Shengju Ding[b], Guqiao Ding[b]*, Xiaoming Xie[a,b]

Rapid thermal exfoliation/reduction of graphite oxide is a fast and easy method among the oxidation-reduction approaches for graphene synthesis. In this research, we firstly demonstrated that graphene can be obtained with a surface area of 550 to 700 m^2/g and a yield of approximately 50% through one-step rapid thermal treatment in air from 450 to 550 °C, without vacuum or protective gas through a self-
10 protection process. Then, we further demonstrated the effective two-step thermal annealing to significantly improve the C/O ratio from c. 7.3 to 25.9 in air at the relatively low temperature of 600 °C. The smart self-protecting and enhanced-oxygen-removal mechanisms were discussed.

Introduction

There are several approaches for the large-scale synthesis of
15 graphene, including oxidation-reduction, liquid exfoliation, intercalation-exfoliation, and substrate-free chemical vapour deposition [1]. Oxidation-reduction is an important approach since the water-soluble intermediate graphene oxide has been proven to be useful, and the reduced product can be just a single
20 or a few atomic layers in thickness with a Brunauer-Emmett-Teller (BET) surface area over 500 m^2/g [2]. Rapid thermal treatment of graphite oxide has attracted considerable attention since the exfoliation and reduction take place at the same time in just several seconds or minutes, and as a result this technique can
25 be developed as a simple, ultrafast, non-chemical, reproducible method for the reduction of graphene oxide [2]. However, the oxidation-reduction method presents the shortcoming of a high oxygen content, i.e., a low C/O ratio, caused by strong oxidation and incomplete reduction, which will result in poor mechanical
30 properties, and low thermal/electronic conductivities [3,4].

To efficiently remove oxygens and produce graphene with a higher C/O ratio, a reducing environment, high vacuum and/or high temperature are generally required [5]. We list the data from the literatures on thermally reduced graphene under a wide
35 temperature range, in N$_2$, Ar, or Ar/H$_2$, with or without vacuum, in Table S1 [6-13]. It was clear that high C/O ratios (i.e. over 25) can only be achieved at temperatures over 1000 °C under Ar or H$_2$ protection, or high vacuum. All the C/O ratios were lower than 15 at temperature below 1000 °C whether under vacuum or
40 reductive gas. When the temperature was lower than 650 °C, the most reduced graphene had a C/O ratio of less than 10. Obviously, the high temperature, H$_2$ atmosphere, or high vacuum will lead to high cost. A simple, low-temperature, and atmospheric pressure based thermal reduction approach will satisfy the urgent demand
45 of large scale graphene synthesis with a controllable C/O ratio and low cost.

Here, we firstly demonstrated that graphene can be made with a

BET surface area of 550-700 m^2/g and a yield of c. 50% by a one-step rapid thermal treatment in air at 450-550 °C, without vacuum
50 or protective atmosphere through a smart self-protection set-up. Then, we further demonstrated the effectiveness of a two-step thermal annealing process to improve the C/O ratio from c. 7 to 25.9 in air at a temperature of 600 °C. The self-protecting and oxygen-removing mechanisms were proposed and discussed on
55 the basis of experimental evidences. The graphene powder had good quality, as evidenced by several measurements, the high C/O ratio, better performance in Li-ion battery. This simple and low-cost approach will facilitate the large-scale fabrication of high-quality graphene powder.

Materials and methods

Reagents

Natural graphite powder, with a lateral size of 45 μm (325 mesh), and sodium chlorate (AR, ≥ 99.0%), was supplied by Aladdin. Concentrated sulphuric acid (95-98%) and nitric acid
65 (65-68%) were obtained from Shanghai Lingfeng Chemical Reagent Company, China. Lithium iron phosphate (LiFePO$_4$) was bought from Süd-Chemie Company, Germany. KS-6 conductive graphite and Super-P carbon black were supplied by TIMCAL Graphite. Poly (vinylidene fluoride) (PVDF) and N-methyl-2-
70 pyrrolidene (NMP) were bought from Alfa Aesar and Aladdin, respectively.

Preparation of graphite oxide

The graphite oxide was obtained by the Staudenmaier method. For this method, graphite (5.0 g) was put into a mixture of
75 concentrated nitric acid (57 ml) and sulphuric acid (107 ml). The mixture was controlled within 0-10 °C and stirred for 30 minutes. Then, sodium chlorate (60.0 g) was added slowly to the mixture. After sodium chlorate addition, the mixture was kept at 15 °C for five hours' reaction. Then, the mixture was filered to obtain the
80 product slurry. The slurry was repeatedly washed with deionised water until the pH value was neutral. Then, the neutral slurry was

freeze-dried for 3 days, and the dried sample was placed in a vacuum oven at 60 °C for 24 hours.

Thermal exfoliation and reduction of graphite oxide

5 The first rapidly thermal exfoliation/reduction was performed in air in a self-designed crucible. A steel or graphite cuboidal box, 160 mm × 150 mm × 60 mm, with a lid was used as the container (see Fig. S1). The wall thickness of the box was 0.1-0.2 mm to allow for efficient heat conduction. When the furnace was heated to the target temperature, the container, with 1.0 g graphite oxide
10 therein, was put into the furnace as soon as possible, and treated for 10 s to 2 min. Black and fluffy graphene was obtained in the container, as shown in Fig. S1. For the two-step thermal annealing, the sample was first thermally reduced at 600 °C in air and cooled in air or Ar for 24 hours, it was thermally annealed for
15 the second time at 600 °C in air or Ar. In order to have a good repetition, the amount of sample is just 1.0 g with the same container, and during all the annealing process the lid was on the container for both the one-step and two-step annealing.

Characterisation

20 Scanning electron microscopy (SEM S4700, Hitachi Inc.) was used to image the morphology of the samples. Transmission Electron microscopy (TEM) was undertaken on H-8100 EM (Hitachi, Tokyo, Japan) with an accelerating voltage of 200 kV. X-ray photoelectron spectroscopy (XPS) measurements were
25 carried out using a Thermo ESCALAB 250Xi spectrometer. Raman spectroscopy was performed using a Thermo Fisher DXR Raman Microscope, with an excitation laser wavelength 532 nm. X-ray diffraction (XRD) patterns were obtained from an X-Ray Diffractometer (Bruker D8 ADVANCE) with a monochromatic
30 source of Cu Kα1 radiation (λ = 0.15405 nm) at 1.6 kW (40 kV, 40 mA). The specific surface area was determined by V-Sorb 2800P (Gold APP Instruments Corporation, China) through the BET method. The electrical properties were measured by a Hall measurement system (Accent HL5500). The test samples were
35 prepared by a tablet machine (FW-4, Tianjin TianGuang Optical Instruments Corporation, China) with 100 mg graphene pressed under a pressure of 20 MPa for 10 minutes. The diameter and thickness of the thin flakes were 13.15 mm and 0.6 mm, respectively.

40 **Cell fabrication and electrochemical measurements**

The fabrication method used for the positive electrode was similar to that reported elsewhere [14-15]. It was prepared by coating conductive slurry onto Al foil, with a thickness of 100 μm, by trap-cast process, then the sample was dried at 120 °C for 2
45 hours in a vacuum oven [16]. The components of the slurries were: $LiFePO_4$ (91.7 wt%), a mixture of KS-6 conductive graphite (1.5 wt%) and Super-P carbon black (3.5 wt%), the PVDF (3.3 wt%), and N-methyl-2-pyrrolidene (NMP). The electrodes for the test samples were prepared by the same method
50 using 1 wt% graphene (one-step and two-step annealed) to replace the KS-6 conductive graphite (0.3 wt%) and Super-P carbon black (0.7 wt%). The cells were assembled in a 2032 button-type cell in an argon-filled glove box, and then stewed for 24 hours before electrochemical measurements.

55 Electrochemical impedance spectroscopy (EIS) of cells was undertaken on an electrochemical workstation (CHI660) over the frequency range from 100 mHz to 100 kHz. The charge/discharge performances were measured using a Small (micro) Current

Device (CT2001A, Wuhan LAND Electronics). For the first
60 cycle, the button-type cells were charged at a constant current density of 0.1 C-rate until 4.1 V (vs Li^+/Li). Next, 4.1 V was continuously applied until a current density of 0.05 C-rate was reached, and they were then discharged at 0.1 C-rate until a voltage of 2.0 V was realised. We repeated this charge/discharge
65 cycle (2.0-4.1 V) five times at a current density of 0.1 C-rate. The current density was changed to 0.5, 1 C-rate and the same charge/discharge cycle were repeated for five times. Finally, the specific capacity-cycle times spectroscopy and voltage-specific capacity spectroscopy data were obtained.

70 # Results and discussion

First step rapid thermal exfoliation/reduction of graphite oxide in air

The first rapidly thermal annealing (at 250-1050 °C) was produced in air without any protective or reductive gases for 10 s
75 to 2 min. A steel box with a lid was used as the container, as shown in Fig. 1 and S1. The graphite oxide was loaded into the box in air, which means that there are some oxygen and nitrogen in the container. It should be emphasized that the atmosphere in the box is dynamic during the whole annealing process due to the
80 gas release.

The graphene yield is listed in Table S2. The value of the graphene yield between 250 and 350 °C are inapplicable because graphite oxide was not exfoliated, or only partially exfoliated. The yield of around 50% at 450 and 550 °C was reasonable due
85 to the c. 30 at.% oxygen content in the precursor graphite oxide (Fig. S2, XPS data for graphite oxide). And as expected, the yield of graphene decreased with increasing of annealing time because of carbon oxidation. At high temperatures of 750 and 850 °C, the yield was very low, and it was found that the annealed samples
90 were slowly burning when the lid was removed. At 950 and 1050 °C for 30 s, the samples burned fiercely in air upon removal of the lid, and it was thus difficult to obtain graphene and the value of the graphene yied.

95
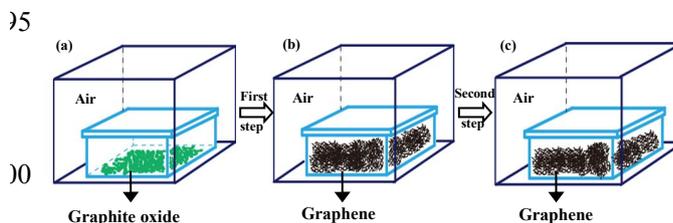
Fig. 1 - A sketch map of the one-step and two-step thermal annealing: (a) The container with graphite oxide was put into the furnace,(b), the
105 graphite oxide powder underwent an approximate 500-fold volumetric expansion during the first annealing , (c) after cooling in air, the container was returned into the furnace for second annealing in air.

Table 1 shows the BET specific surface of graphene, which
110 was obtained by thermal exfoliation / reduction at 450-850 °C in air without protecting gases. Compared with the literatures (Table S3), the BET values of 500-700 m^2/g of graphene prepared at 450 and 550 °C was very good. The typical SEM, TEM, and HRTEM images, as well as the XPS data, for graphene obtained at 550 °C

for 30 s are presented in Fig. S3. The oxygen content of the graphene is about 12 at. % according to the XPS data. The C/O ratio of 7.3 was comparable to the results obtained under vacuum or Ar/H₂ as listed in Table S1 [4, 9, 12]. All of these data directly

5 confirm the formation of few-layered graphene powder through one-step rapidly thermal exfoliation and reduction of graphite oxide in air at low temperatures, and the graphene obtained in air did not exhibit any obvious shortcomings compared with that obtained by thermal annealing in H₂, or under high vacuum. The

10 mechanism of successful one-step annealing in air will be discussed and confirmed later. Considering the yield and cost, the temperature range of 450 to 650 °C is suitable for the one-step thermal annealing of graphite oxide in air.

15 Table 1 BET data of graphene obtained at 450-850 °C for 10-120 s in air

	10 s	30 s	60 s	120 s
450 °C	569.9	608.0	703.5	677.7
550 °C	584.8	612.1	706.8	730.2
650 °C	644.9	613.1	596.0	634.1
750 °C	626.1	815.8	833.8	755.3
850 °C	669.0	789.1	771.9	797.6

Two-step annealing to improve the C/O ratio

Table 2 Experimental details and XPS data

Sample No.	Steps	Temp (℃)	Time (min)	Conditions	C (at.%)	O (at.%)	C/O ratio
1#		600	0.5	Air	85.66	12.63	6.8
2#	one -step	600	5	Air	85.40	12.91	6.6
3#		600	15	Air	83.48	15.19	5.5
4#		600	0.5	Sample 1#; annealing in air	87.93	11.30	7.8
5#	two -step	600	5	Sample 1#; annealing in air	95.24	4.21	22.6
6#		600	15	Sample 1#; annealing in air	95.75	3.69	25.9
7#	two- step	600	15	Condition*	85.38	12.79	6.68

Conditions*: After annealing in air for the first time as samples 4, 5, 6#, the
20 second step annealing was conducted in a tube furnace with a continuous 100 sccm Ar flow, a 20 °C/min temperature increase rate, and 10 °C/min temperature decrease rate.

Although we synthesised few-layered graphene in air at low
25 temperatures with a high surface area, its oxygen content was generally more than 10 at.%, with a C/O ratio of less than 10.0. We tried several approaches to decrease the oxygen content, for example, increasing the rapidly thermal annealing time(samples 1#, 2#, and 3#) and second annealing, as shown in Table 2. We
30 found that it is difficult to further decrease the oxygen content for the one-step annealing, and that the second step annealing in air
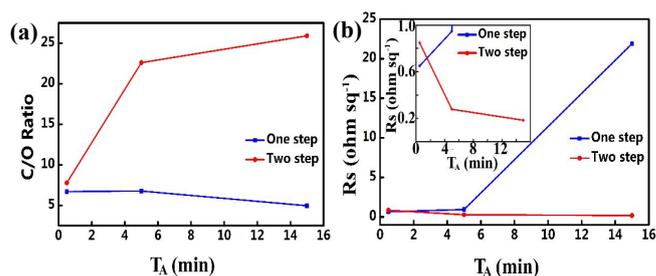
Fig. 2 - The of C/O ratio (a) and surface resistance (b) of graphene obtained through one-step and two-step annealing for different time,
35 Inset in (b) is the high magnification views of surface resistance.

can significantly decrease the oxygen content. The graphite oxide was annealed at 600 °C for 30 s in air for the first time, then cooled for 24 hours, and thermally annealed again for the second
40 time at 600 °C for 30 s to 15 min in air. For a better comparison, we conducted one-step, two-step, and controlled sample tests under the same conditions (see Table 2).

The C/O ratio datas in Fig. 2a represents the obvious difference between the one-step and two-step annealing approaches. As the
45 annealing time increasing in the first step, the C/O ratio decreased from 6.70 to 4.96, while the C/O ratio increased to 22.6 and 25.9 after 5 min and 15 min in the second step, respectively. It was interesting to note that second step annealing can significantly remove containing oxygen groups on the graphene. The higher
50 C/O ratio means fewer defects on the graphene sheets, which was confirmed by conductivity tests, as shown in Fig. 2b. The increase of surface resistance of the long-time one-step annealed graphene may be caused by the carbon oxidation in air.

For further improving the C/O ratio, we did try the three-step
55 annealing. Actually, we got the highest C/O of 45.8, a significant improvement from C/O of 25.9 in the two-step annealing, by treating two-step annealed graphene under 600 ℃ for 5 min in air. However, the repeatability is not acceptable due to partial sample burning.

60 **The mechanism of self-protection**

The ambience change is very important to understand the mechanism. It should be noted at first that the container we used is not sealed, and the gap between container and lid facilitated the gas in and out. Before the first step annealing, the graphite oxide
65 was put into the container with air in it, and during the annealing, the oxygen-containing groups will decompose, and some carbon atoms are oxidized into CO₂ [17-18]. According to the pure carbon weight loss at 500-600 °C (1g precursor of graphite oxide with 65% carbon content, 0.5g reduced graphene oxide with 90%
70 carbon content, the carbon loss 1×0.65-0.5×0.9=0.2g), the total CO₂ release was about 1.2 L at 500 ℃ while the container 0.21 L O₂ and 0.78L N₂ in it since the its total volume is about 1 L. The CO₂ release would consume some oxygen, and extra gas would come out from the container. As a result, the remaining gases in
75 the container should be mainly composed of CO₂. A little O₂ outside the container may come into the container, but its amount should be limited. We proposal the self protection due to the CO₂ release during the annealing and the released CO₂ may be adsorbed on graphene sheet surface to form an inert protecting
80 layer. The TGA measurements (Fig. S4) of graphite oxide and

one-step annealed grpahene in air and N_2 were conducted to understand the decomposition, and to see any difference with and without a container. The fast weight loss of one-step annealed grpahene at around 550 ºC in air can further confirm the importance of the container used to provide a self-protection.

Based on the self-protection mechanism, we also tried to figure out the reason why second annealing improved C/O ratio. After putting a one-step annealed graphene in air for 24 hours, and re-annealing it at the same temperature (Table 2), its C/O ratio was improved significantly. The control samples 7# was studied. After one-step annealing in air in the container, reduced graphene oxide was taken out for 24 hours. The second step annealing was conducted in a tube furnace with a continuous 100 sccm Ar flow, a 20 °C/min temperature increase rate, and 10 °C/min temperature decrease rate. These parameters can ensure the non-oxygen annealing process. But after the second step annealing, the C/O ratio of the control sample 7# was not improved, which meant that the residual oxygen groups cannot be removed if pure Ar was filled, or no oxygen was involved in the second annealing.

To figure out the effect of partial oxygen in the ambience of container, we conducted a lot of XPS measurements to study the surface chemistry of different samples. C 1s and O 1s XPS patterns of samples made using different thermal annealing regimes are shown in Fig. 3. They represent the samples in Table 2 after one-step thermal annealing for 30 s at 600 °C (a, b, sample 1#), one-step thermal annealing for 15 minutes at 600 °C (c, d, sample 3#), and two-step thermal annealing for 15 minutes at 600 °C (e, f, sample 6#). For C 1s XPS patterns, the four peaks indicated the four types of carbon atom in the lattice. The binding energy peaks, located at 284.6, 285.8, 287.8, and 289.3 eV, can be assigned to the non-oxygenated ring C=C/C-C, the hydroxyl and epoxy C-O, the carbonyl C=O, and the carboxylate carbon O=C-O, respectively [5, 6, 9, 19-21]. For the O 1s XPS patterns, there are two peaks located at 531.2 and 533.6 eV, which can be assigned to the C=O and C-O bonds, respectively [6, 9]. For one-step annealing for 30 s and 15 min, there is no significant change in the C1s peaks with a slight increase for C=O in O 1s XPS spectrum. However, when the sample was cooled and reheated to 600 °C for the second time, promotion of the non-oxygenated ring C=C/C-C in the C 1s spectra could be observed in Fig. 3e, and at the same time the proportion of C-O decreased significantly while the carbonyl C=O nearly disappeared. For the O 1s XPS patterns, there are C-O and C=O peaks, and for long-term annealing over 15 min (the first step), the C=O peak increased, and total oxygen content also increased. After second step annealing, the C=O peak decreased. Thus, it was proposed that the oxygen may react with the C-O groups during second step annealing to form C=O groups on the graphene surface, which can then be further converted to COOH groups [6], which are more thermally unstable and can be easily removed at low temperatures.

According to the XPS and other datas, the two-step annealing significantly improve the C/O ratio is mainly caused by the transformation between C-O and C=O, as evinced by the XPS data of Fig. 3. The important transformation from C-O to C=O should be improved by a little bit oxygen, which is the reason why we can get graphene with higher C/O ratio in air under just 600 °C , not in pure Ar.
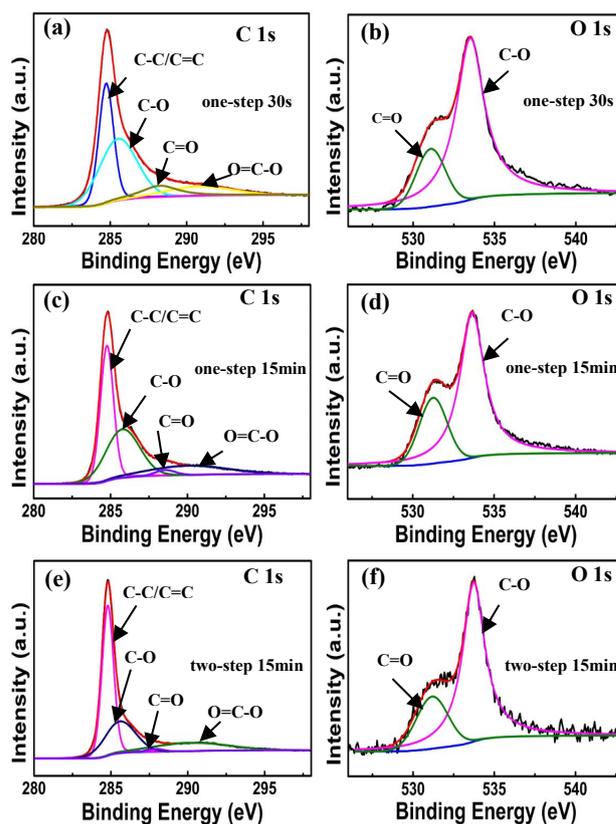
Fig. 3 - XPS C 1s and O 1s spectra of one-step annealed graphene at 600 °C for 30 s (a and b), one-step annealed graphene at 600 °C for 15 minutes (c and d), and two-step annealed graphene at 600 °C for 15 min (e and f).

Good quality graphene obtained by a two-step annealing approach

Fig. 4a shows the XRD patterns of the graphite oxide precursor, the graphene made by one-step rapidly thermal treatment in air, and two-step thermal annealing in air. Compared with graphite oxide, a wide peak ($2\theta = 23.7°$) was seen in the pattern of one-step annealing graphene. According to the formula $n\lambda = 2d\sin\theta$, the interlayer distance was reduced to 3.75 Å due to the elimination of carboxyl groups in the plane and on the edges of the graphene sheets [7]. After the second annealing, the interlayer distance further decreased to 3.45 Å ($2\theta = 25.8°$), closer to 3.35 Å of pristine graphite [22], which indicated that the functional groups among the graphene inter-layers were almost removed.

Furthermore, with the increase of C/O ratio and removal of functional groups, there should be fewer defects on the graphene sheets. Raman spectroscopy is a powerful technique for examining local defects, disorder, and the layer characteristics of graphene. The main features of reduced graphene and graphite oxide in Raman spectroscopy are the G peak (c. 1580 cm^{-1}) assigned to the honeycomb arrangement of sp^2 carbon atoms, and the D peak (c. 1350 cm^{-1}) assigned to the defects or disorder [23]. The intensity ratio of the D and G peaks (I_D/I_G) is usually used to characterise the quality of reduced graphene [7]. Fig. 4b shows the Raman spectra of graphite oxide, one-step graphene, and two-step graphene. The I_D/I_G continuously decreased from 0.966
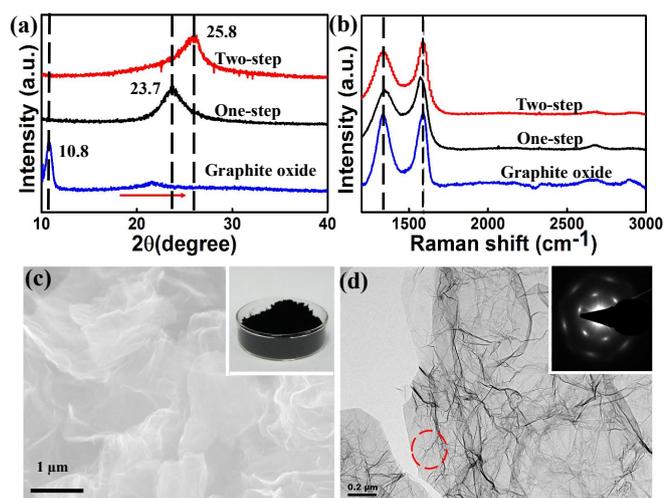
Fig. 4 - The structure and morphology of the samples: (a) XRD and (b) Raman curves of the graphite oxide, one-step annealing in air at 600 °C and two-step annealing in air at 600 °C, (c) SEM and (d) TEM images of the two step annealing in air at 600 °C. The inset in (c) is a digital photo, and the inset in (d) is the SAED pattern of the as-made graphene.

(graphite oxide) to 0.899 (one-step annealed graphene), and finally to 0.864 (two-step annealed graphene), which was consistent with the result of XRD spectroscopy, indicating the decreasing of oxygen groups. We also conducted the Raman mapping to further confirm the uniformity of the samples, as shown in Fig. S5. SEM and TEM measurements were conducted to intuitively reveal the graphene microstructure. As shown in Fig. 4c and 4d, a fluffy, worm-like and transparent morphology was observed. The selected area electron diffraction (SAED) showed perfect hexagonal symmetry and indicated the good staking order of the sp^2 layered structure. All XRD, Raman, SEM, and TEM data confirm the successful synthesis of graphene through this simple thermal treatment in air and low temperatures.

Limitations and Expectations

It should be noted that our approach has some limitations. For example, if the sample is less than 0.1 g in the 1L container, we will get nothing for the one-step or two step annealing since there are too much oxygen and less CO_2 release during the annealing. If there are more than 3.0 g in the 1L container, the rapidly exfoliated graphene will release too much gas, and the resulted graphene has very large volume, which in turn leads to the fluffy powder out of the container. Especially for the second step annealing, it is hard to well control or repeat the experiments since the CO_2 release will be much less than that during the first annealing when treating 1g sample in the 1L container.

However, we have repeated the one-step annealing with 1g sample for more than 100 times. And the process itself, as well as properties of obtained graphene, is repeatable. Furthermore, more than 10 g graphene with higher C/O ratio was also obtained through the two-step annealing. Although it is still a not well control approach, it gives some lights for achieving reduced graphene with less oxygen defects under lower temperatures.

Application in Li-ion batteries as an additive
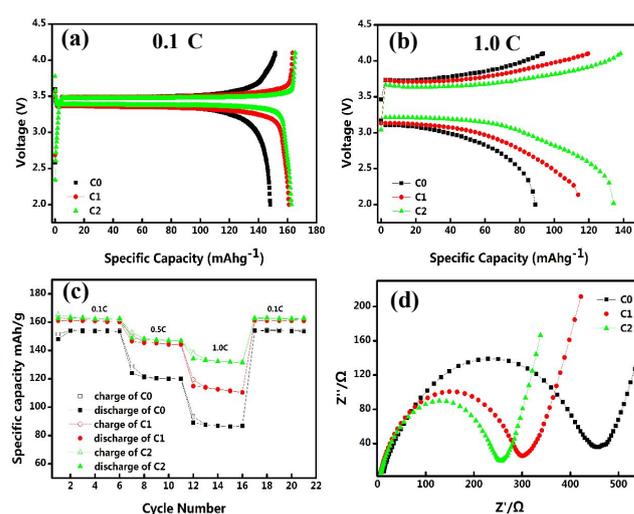
Fig 5. - The electrochemical characteristics of Li ion battery cells loaded with LiFePO$_4$ without graphene (C0), LiFePO$_4$ with one-step (C1) and two-step (C2) thermally annealed graphene. The voltage profiles for the first cycle charging and discharging with a 0.1 C rate (a) and 1.0 C rate (b) of the Li ion battery cells, (c) the charge and discharge rate capability at different charge/discharge rates for the Li ion battery cells, (d) electrochemical impedance spectroscopy of the Li ion battery cells.

It has been established that two-step thermally annealed graphene had a higher C/O ratio and conductivity. So there would be an important application for this graphene as a conductive additive in Li-ion batteries [24]. Fig. 5 shows the electrochemical performances of Li-ion battery cells (loaded with LiFePO$_4$ without graphene, and with LiFePO$_4$ with one-step and two-step thermally annealed graphene). The cells with the addition of two-step thermally annealed graphene exhibited a higher discharge capacity than that in the control experiment and that using one-step thermally annealed graphene at a 0.1 C-rate (Fig. 5a): the value of 164 mAhg^{-1} was as high as the reported values of 120-160 mAhg^{-1} for commercially available, or synthetic, LiFePO$_4$ materials in research laboratories [25-28]. Especially at the 1.0 C rate (Fig. 5b), specific discharge capacity values of those cells with two-step and one-step thermally annealed graphene and their control experiment were 135, 114, and 90 mAhg^{-1}: the advantage bestowed by using two-step thermally annealed graphene was clear.

The rate performances of the cells are shown in Fig. 5c. As expected, with the increase of discharge rate, no cell could sustain the high discharge current (fast Li$^+$ intercalation) and thus the capacity faded very quickly. However, the cells loaded with two-step thermally annealed graphene still retaines the high specific discharge capacity value. This suggests that the two-step thermally annealed graphene has better electrical properties than its one-step counterpart. In addition, electrochemical impedance spectroscopy (EIS) of the cells also confirmed that the impedance of two-step thermally annealed graphene was approximately half that of one-step thermally annealed graphene (Fig. 5d). The graphene sheets acted as a flexible two-dimensional carbon network support for homogeneous anchoring of LiFePO$_4$, and the two-step thermally annealed graphene had better electrical

conductivity and fewer defects, contributing to its better battery performance. In turn, the superior Li$^+$-battery performance further validated the supposition that the structure and properties of graphene were restored and improved by an increased C/O atom 5 ratio.

Conclusion

An efficient, rapidly thermal treatment approach to graphene synthesis in air and at low temperatures was demonstrated. A high C/O ratio of up to 25.9 was realised by two-step annealing in 10 air and at a relatively low temperature of 600 °C. The smart, self-protecting and oxygen-removing mechanism are based on the adsorption/desorption of generated CO_2 and gas exchange between the adsorbed CO_2 and oxygen in the container. The graphene with a higher C/O ratio was used as a conductive 15 additive in the electrode of a Li-ion battery where it was demonstrated a higher performance than graphene with a lower C/O ratio. The findings of this research will help the community to better understand the oxygen-removal process on graphite oxide or graphene oxide, and may pave the way for large-scale 20 graphene powder synthesis and for further improvement of the quality of graphene.

Associated content

Supporting information available

Table summarising the C/O ratio of graphene. Experimental 25 details, yield at different temperatures, XPS survey spectrum, BET, SEM, and TEM of one-step annealed graphene. This material is available free of charge over the Internet.

Acknowledgements

Notes and references

35 *a School of Physical Science and Technology, ShanghaiTech University, Shanghai 200031, P.R. China*
b State Key Laboratory of Functional Materials for Informatics, Shanghai Institute of Microsystem and Information Technology, Chinese Academy of Science, Shanghai 20050, P. R. China
40 *Corresponding author: Prof. Guqiao Ding, gqding@mail.sim.ac.cn*

References

1 W. C. Ren, H. M. Cheng, *Nat Nanotech*, 2014, **9**, 726.
2. M. J. McAllister, J. L. Li, D. H. Adamson, H. C. Schniepp, A. A. Abdala, J. Liu, M. Herrera-Alonso, D. L. Milius, R. Car, R. K. 45 Prud`homme, *Chem. Mater.*, 2007, **19**, 4396.
3. C. Botas, P. Álvarez, B. Blanco, R. Santamaría, M. Granda, M. D. Gutiérrez, F. Rodriguez-Reinoso, R. Menendez, *Carbon*, 2013, **52**, 476.
4. C. Punckt, F. Muckel, S. Wolff, I. A. Aksay, C. A. Chararin, G. 50 Bacher, W. Mertin, *Appl Phys Lett*, 2013, **102**, 023114.
5. S. F. Pei, H. M. Cheng, *Carbon*, 2012, **50**, 3210.
6. L. L. Geng, S. J. Wu, Y. C. Zou, M. J. Jia, W. X. Zhang, W. F. Yan, G. Liu, *J Colloid Interf Sci*, 2014, **42**, 171.
7. D. Y. Wan, C. Y. Yang, T. Q. Lin, Y. F. Tang, M. Zhou, Y. J. Zhong, 55 F. Q. Huang, J. H. Lin, *ACS nano*, 2012, **6**, 9068.
8. H. Park, H. Ahn, Y. Chung, S. B. Cho, Y. S. Yoon, D. J. Kim, *Mater. Lett.*, 2014, **136**, 164.
9. O. Akhavan, *Carbon*, 2010, **48**, 509.
10. S. H. Ha, Y. S. Jeong, Y. J. Lee, *ACS Appl. Mater. Inter.*, 2013, **5**, 60 12295.
11. D. X. Yang, A. Velamakanni, G. Bozoklu, S. Park, M. Stoller, R. D. Piner, S. Stankovich, I. Jung, D. A. Field, C. A. Ventrice, R. S. Ruoff, *Carbon*, 2009, **47**, 145.
12. Z. S. Wu, W. C. Ren, L. B. Gao, B. L. Liu, C. B. Jiang, H. M. Cheng, 65 *Carbon*, 2009, **47**, 493.
13. H. C. Schniepp, J. L. Li, M. J. McAllister, H. Sai, M. Herrera-Alonso, D. H. Adamson, R. K. Prud`homme, R. Car, D. A. Saville, I. A. Aksay, *J Phys Chem B*, 2006, **110**, 8535.
14. W. K. Kim, W. H. Ryu, D. W. Han, S. J. Lim, J. Y. Eom, H. S. Kwon, 70 *ACS Appl. Mater. Inter.*, 2014, **6**, 4731.
15. L. Zhang, S. Q. Wang, D. D. Cai, P. C. Lian, X. F. Zhu, W. S. Yang, H. W. Wang, *Electrochim Acta*, 2013, **91**, 108.
16. L. H. Hu, F. Y. Wu, C. T. Lin, A. N. Khlobystov, L. J. Li, *Nat Commun*, 2013, **4**, 1687.
75 17. J. I. Paredas, S. Villar-Rodil, P. Solis-Fernandez, A. Martinez-Alonso, J. M. D. Tascon, *Langmuir*, 2009, **25**, 5957.
18. W. F. Chen, L. F. Yan, P. R. Bangal, *Carbon*, 2010, **48**, 1146.
19. Y. Yamada，K. Murota, R. Fujita, J. Kim, A. Watanabe, M. Nakamura, S. Sato, K. Hata, P. Ercius, J. Ciston, C. Y. Song, K. Kim, 80 W. Regan, W. Gannett, A. Zettl, *J Am Chem Soc*, 2014, **136**, 2232.
20. X. B. Li, S. W. Yang, J Sun, P. He, X. P. Pu, G. Q. Ding, *Synthetic Met*, 2014, **194**, 52.
21. X. B. Li, S. W. Yang, J. Sun, P. He, X. G. Xu, G. Q. Ding, *Carbon*, 2014, **78**, 38.
85 22. O. C. Compton, B. Jain, D. A. Dikin, A. Abouimrane, K. Amine, S. B. T. Nguyen, *ACS nano*, 2011, **5**, 4380.
23. A. C. Ferrari, J. C. Meyer, V. Scardasi, C. Casiraghi, M. Lazzeri, F. Mauri, S. Piscanec, D. Jiang, K. S. Novoselov, S. Roth, A. K. Geim, *Phys. Rev. Lett.*, 2006, **97**, 187401.
90 24. G. Kucinskis, G. Bajars, J. Kleperis, *J Power Sources*, 2013, **240**, 66.
25. J. L. Yang, J. J. Wang, D. G. Wang, X. F. Li, D. S. Geng, G. X. Ling, M. Gauthier, R. Y. Li, X. L. Sun, *J Power Sources*, 2012, **208**, 340.
26. Y. Shi, S. L. Chou, J. Z. Wang, D. Wexler, H. J. Li, H. K. Liu, Y. P. Wu, *J Mater Chem*, 2012, **22**, 16465.
95 27. B. T. Zhao, X. Yu, R. Cai, R. Ran, H. T. Wang, Z.P. Shao, *J Mater Chem*, 2012, **22**, 2900.
28. C. M. Doherty, R. A. Caruso, B. M. Smarsly, P. Adelhelm, C. J. Drummond,*Chem.Mater.*,2009,**21**,5300.